Journal of Catalysis 410 (2022) 320–332

Contents lists available at ScienceDirect

Journal of Catalysis

journal homepage: www.elsevier.com/locate/jcat

Controlling diffusion resistance, selectivity and deactivation of ZSM-5 catalysts by crystal thickness and defects

Jonas Hedlund [a,*], Ming Zhou [a,*], Abrar Faisal [a,1], Olov G.W. Öhrman [a,c], Valeria Finelli [b], Matteo Signorile [b], Valentina Crocellà [b], Mattias Grahn [a]

[a] Chemical Technology, Luleå University of Technology, 971 87 Luleå, Sweden
[b] Department of Chemistry, NIS and INSTM Reference Centre, Università di Torino, Via G. Quarello 15, I-10135 and Via P. Giuria 7, I-10125 Torino, Italy
[c] RISE Energy Technology Center, Box 726, 941 28 Piteå, Sweden

ARTICLE INFO

Article history:
Received 29 November 2021
Revised 4 April 2022
Accepted 14 April 2022
Available online 25 April 2022

Keywords:
H-ZSM-5
Defects
Gasoline
Deactivation
MTG

ABSTRACT

A systematic investigation of two sets of defect free and defective ZSM-5 crystals with controlled thickness (T) between 30 and 400 nm and of their performances in methanol conversion was reported for the first time in the present work. The defect free ZSM-5 crystals with a thickness of 35 nm are by far the smallest ever reported and displayed superior activity, stability and selectivity to slower diffusing compounds, which resulted in high yield of e.g. gasoline and the 1,2,4-trimethylbenzene isomer with high octane number, as compared to the other studied catalysts. Almost only products forming in the zeolite pores were detected and consequently, the external surface must be nearly inactive. Strong correlations between T and deactivation rate were observed. Thick crystals deactivated much faster than thin crystals, probably due to formation of carbon species in the zeolite pores, which results in pronounced percolation effects and faster deactivation of the former. At comparable thickness, crystals with defects deactivated much faster than defect free crystals, due to formation of additional small molecular coke species in the former. Strong correlations between T and selectivity were also observed and assigned to control of diffusion resistance by crystal thickness.

1. Introduction

Methanol can be converted to hydrocarbons (MTH) using an acid catalyst. First, methanol is dehydrated to dimethyl ether, which results in a mixture of methanol, dimethyl ether and water. In the next step, this mixture can be reacted further, preferably on a zeolite catalyst, to form olefins and gasoline. If an 8-ring zeolite with small pores with a diameter of about 4 Å such as H-SAPO-34 is used, predominantly olefins are formed, and the process is denoted methanol to olefins (MTO). If a 10-ring zeolite such as H-ZSM-5 with slightly larger pores with a diameter of about 5.5 Å is used, also aromatic compounds are formed, and the process is denoted methanol to gasoline (MTG). This process is a good candidate for the synthesis of renewable gasoline by gasification of biomass, followed by methanol and gasoline synthesis. The recent state of the art on the MTH reaction using zeolites has been described in several articles [1–4].

In the MTG reaction, H-ZSM-5 is producing a range of hydrocarbons including ethylene, propylene, heavier alkanes and alkenes and aromatics. A propylene/ethylene carbon ratio of 2–3 is typically observed. The aromatic compounds are comprising a large fraction of xylene isomers, valuable raw materials for the petrochemical industry, and also wanted compounds in gasoline as the octane number is high. The most prominent aromatic compound is 1,2,4-trimethyl benzene (TMB), also known as pseudocumene. Similarly to the xylenes, 1,2,4-TMB is a wanted compound in gasoline, as it has a high octane number. However, the heaviest (aromatic) compound produced in any quantity by ZSM-5 is the (in gasoline) unwanted compound 1,2,4,5-tetramethylbenzene, also known as durene. Since it has a high melting point of 79 °C, it may foul the fuel system in an engine, especially in cold climate, but in warmer climates, up to about 4% durene is acceptable in gasoline fuel. In the MTG process, most of the durene is converted by isomerisation in the heavy gasoline treating unit and the gasoline is fully compatible with conventional gasoline [5].

* Corresponding authors.
E-mail addresses: jonas.hedlund@ltu.se (J. Hedlund), ming.zhou@ltu.se (M. Zhou).
[1] Department of Chemical Engineering, COMSATS University Islamabad, Lahore Campus, Lahore, Pakistan.

https://doi.org/10.1016/j.jcat.2022.04.013
0021-9517/

Deactivation of zeolite catalysts due to coke formation is a relevant issue in industrial processes, and consequently, deactivation in the industrially important MTH reaction has been studied and reported in numerous research papers as summarized by Olsbye et al. [1]. In short, it is accepted that coke formation in ZSM-5 is a result of initial formation of alkylated mono- and polycyclic aromatics near the channel intersections in the zeolite pores. This is followed by formation of surface coke from polycyclic compounds near the pore openings, which results in a graphitic layer, which eventually block the access to the pores. Recent work indicated that these extended carbon species may be amorphous carbon with disordered graphitic domains, possibly with contribution from H-containing species [6].

Of particular importance for the present work are reports on coke formation and deactivation by Barbera [7], Weckhuysen [8], Froment [9] and Holmen [10] as described in the following. Barbera et al. [7] systematically investigated a large number of ZSM-5 catalysts, with particle size of 100 and 300 nm for the methanol to hydrocarbons reaction. It was concluded that internal framework defects are crucial for deactivation of the catalysts. Moreover, it was shown that these internal framework defects, i.e. silanol nests, can be probed by FTIR spectroscopy. It was also clearly illustrated that the catalyst activity is linearly correlated with the number of active sites.

In a recent study, Weckhuysen et al. [8] used atom probe tomography to show that coke was present as agglomerates that spanned length scales from tens of nanometers to atomic clusters with a median size of 30–60 carbon atoms in ZSM-5 crystals partially deactivated during the MTH reaction. These atomic clusters are denoted "carbon species" in the present work.

Froment and co-workers reported models for deactivation of zeolite catalysts by percolation effects already in 1993 [9]. Only a few years later, Holmen et al. observed experimentally that 0.25 μm SAPO-34 crystals deactivated slower than 2.5 μm crystals during methanol conversion. By using the Monte Carlo method and percolation theory, it was shown that the reduced reaction rate could be a result of reduced diffusivity caused by percolation effects due to coke formation in the catalyst. A more significant diffusion limitation was observed for larger crystals, and hence these deactivated faster [10].

We have previously evaluated nano-sized (120 nm) as well as mesoporous ZSM-5 crystals for conversion of methanol to gasoline and reported that both deactivated slower as compared to conventional ZSM-5 crystals [11,12]. In later work, we also improved the conventional synthesis procedure, which results in very well defined mesoporous ZSM-5 crystals [13].

Chen et al [14] systematically studied the influence of crystal size on the methanol to olefin reaction over SAPO-34 crystals. The crystal size was varied in the range 0.25–2.5 μm. Somewhat surprising, the 0.25 μm crystals gave high yield of DME, but low olefin yield, while the 0.4–0.5 μm crystals gave the largest olefin yield, while the largest crystals gave lower methanol conversion and lower olefin yield and deactivated faster. Also, the selectivity to different olefins was independent of the crystal size at relatively low coke contents. Faster deactivation of larger SAPO-34 crystals has been observed in later work [15].

As early as in 2009, unilamellar MFI zeolite has been evaluated in the methanol to gasoline reaction [16] The thickness of each lamella is only 2 nm in the *b*-direction. It was shown that the unilamellar zeolite was deactivating much slower as compared to "conventional" ZSM-5 zeolite purchased from Zeolyst. However, only the methanol conversion and coke formation was reported, no information on selectivity was disclosed. The faster deactivation of the conventional zeolite was ascribed to formation of coke in the micropores. On the unilamellar catalysts, mostly external coke was detected. Although the authors did not point it out, formation of internal coke in unilamellar zeolite catalysts will have little or no effect on the activity, since the diffusion path is too short and no percolation effects will occur.

Later, Bleken et al [17] prepared ZSM-5 nanosheets and evaluated the catalytic performance in the MTH reaction. It was reported that the nanosheet had similar selectivities, however with the largest difference that a higher C_3/C_2 carbon ratio was observed, as compared to regular crystals.

ZSM-5 zeolite is conventionally prepared using hydroxide ions as mineralizing agent, and consequently, the pH of the synthesis mixture is high. However, it is known that non-bridging ≡Si-OH defects form at these conditions [18]. ZSM-5 zeolite can also be prepared at near neutral pH using fluoride ions as mineralizing agent, which results in a zeolite with less defects [18]. At these conditions, the nucleation rate is lower, and the growth rate is higher, and consequently, it is possible to prepare several μm large crystals using fluoride as mineralizing agent. However, for catalysis applications, small crystals are needed, and until now, reports on preparation of small ZSM-5 crystals using the fluoride route are scarce.

Bleken et al [19] prepared large ZSM-5 crystals using both the hydroxide and the fluoride route with the aim to optimize the catalyst for high propylene yields. The catalysts were evaluated for the MTO reaction at 350 °C. The best catalyst was ZSM-5 crystals with a length of 15–20 μm with a Si/Al ratio of 53 prepared using the fluoride route. A propylene/ethylene carbon ratio as high as > 5 was observed. This high ratio was tentatively ascribed to the low density of strong acid sites in combination with a long diffusion pathway and few defects.

However, we point out that a long diffusion pathway should of course favor the lighter compound, resulting in a low propylene/ethylene ratio. This is shown by the results in the present work as will be discussed below.

Qin et al. [20] prepared small ZSM-5 crystals grown in fluoride medium, by using seeds grown in hydroxide medium and reported that crystals with sizes below 200 nm could be obtained. It was also shown that a catalyst prepared in fluoride medium was more active and deactivated slower than a sample prepared using hydroxide medium during methanol conversion.

We have reported the preparation of small silicalite-1 (the aluminium free form of ZSM-5) crystals with a thickness of 10 nm in fluoride medium [21,22] without using seeds prepared in hydroxide medium. Recently, we showed that ZSM-5 crystals with a thickness of 100 nm prepared in fluoride medium showed significantly longer catalytic lifetime before deactivation by coke formation in the MTH reaction as compared to ZSM-5 crystals with quite similar morphology and acid site population but prepared using conventional synthesis at high pH [23]. The much slower deactivation of the catalyst prepared in fluoride medium was assigned to a lower density of internal defects. It was also shown that less molecular coke species formed at this less defective catalyst synthesized in fluoride medium, likely due to the absence of enlarged cavities/channels. Consequently, deposition of an external layer of bulk coke should cause the deactivation of the ZSM-5 catalyst synthesized in fluoride medium and in the defective ZSM-5 catalyst synthesized at high pH, the additional molecular coke species that forms inside the crystals should be the reason for the much faster deactivation.

In the present work, we report how small ZSM-5 crystals with controlled thickness down to 35 nm, the lowest ever reported, can be prepared entirely in fluoride medium by using silicalite-1 crystals as seeds. We show that these crystals are excellent catalysts for methanol conversion, giving high yield of gasoline. The results are compared with data from ZSM-5 crystals with the same thickness and similar Si/Al ratio prepared using hydroxide as mineralizing agent. For the first time, a systematic investigation on the

influence of crystal thickness and the presence or absence of defects on the catalytic properties of H-ZSM-5 during methanol conversion is reported.

2. Experimental section

2.1. Preparation of defect free silicalite-1 seed crystals

Defect free silicalite-1 seed crystals were prepared at near neutral pH using fluoride as mineralizing agent in a similar fashion as previously reported.21 First, a clear solution was prepared by shaking a mixture of 24.98 g tetraethoxysilane (TEOS, >98 %, Merk) and 21.95 g tetrapropylammonium hydroxide (TPAOH, 40 %, Sigma) for 24 h in a 100 mL PE bottle. In the next step, some of the water and all ethanol were removed using a rotary evaporator, after which a thick clear gel was obtained. A small amount of distilled water (about 15 g) was added under stirring and a clear solution was obtained again. Then, nucleation was carried out by keeping the clear solution at 60 °C for 6 days in a PE bottle. In the next step, the clear solution was cooled to about 4 °C and then, an equimolar amount (to TPAOH) of hydrofluoric acid (38–40 wt%, Merck) about 2.22 g was added quickly under vigorous stirring. After about 10 s, a very viscous clear gel formed. The molar ratio of this clear gel was 9 TPAF: 25 SiO_2: 300 H_2O and the pH was 6.3. Finally, the gel was hydrothermally treated at 60 °C for 24 h in the bottle. The crystals obtained from this preparation are denoted as S1.

2.2. ZSM-5 crystals with thicknesses of ca 100 and 200 nm grown in fluoride medium using TPA as structure directing agent

ZSM-5 crystals with thickness of ca 100 nm with twin-crystals on (010) faces were grown using the S1 seed crystals by hydrothermal treatment in a clear gel with a Si/Al ratio of 30 using tetrapropylammonium ions originating from Tetrapropylammonium bromide (TPABr, 98%, Sigma) as template, aluminium sulfate ($Al_2(SO_4)_3{\cdot}18H_2O$, ≥97%, Sigma) as aluminium source. After shaking and hydrolyzing the initial 30 g reactants for 24 h in a 100 mL PE bottle, 0.18 g S1 seeds were added to the clear synthesis solution, and the suspension was vigorously shaken for 1 h, then cooled to 4 °C. In the next step, NH_4F was added quickly in an equimolar amount to SiO_2 under stirring. After about 10 s, a viscous white gel formed. The molar composition of the gel was 1SiO_2: 0.08TPABr: 1.0NH_4F: 0.015 $Al_2(SO_4)_3$: 20 H_2O (the seed crystals are omitted).

ZSM-5 crystals with thickness of ca 200 nm with twin-crystals on (010) faces were grown using the S1 seed crystals by hydrothermal treatment in a clear gel with a Si/Al ratio of 30 using tetrapropylammonium ions originating from tetrapropylammonium hydroxide (TPAOH 40% solution in water, Sigma) as template, aluminium isopropoxide (≥98%, Sigma) as aluminium source. After shaking and hydrolyzing the initial 30 g reactants for 24 h in a 100 mL PE bottle, 0.18 g S1 seeds were added to the clear synthesis solution, and the suspension was vigorously shaken for 1 h, then cooled to 4 °C. In the next step, HF was added quickly in an equimolar amount to TPAOH under stirring. After about 10 s, a very viscous white gel formed. The molar composition of the gel was 12TPAF: 25SiO_2: 0.417Al_2O_3: 500H_2O: 2.5i-PrOH: 100EtOH (the seed crystals are omitted).

Both gels for the synthesis of 100 and 200 nm thick ZSM-5 with seeds were respectively hydrothermally treated at 175 °C for 48 h in 50 mL Teflon lined autoclaves. The ZSM-5 crystals prepared in high yield were recovered by centrifugation and dispersion in distilled water for 4 times and freeze-dried.

2.3. ZSM-5 crystals with thicknesses of ca 35, 105 and 253 nm grown in fluoride medium using TEAF (F35, F105 and F253)

ZSM-5 crystals with thicknesses of ca 35, 105 and 253 nm without twin crystal on (010) faces were grown using the S1 seed crystals by hydrothermal treatment in a clear gel with a Si/Al ratio of 30 using tetraethylammonium ions originating from tetraethylammonium hydroxide (TEAOH, 35 %, Sigma) as template. At first, 9.24 g TEAOH 35 % solution was mixed with 10 g H_2O and 0.31 g aluminium isopropoxide in a 100 mL PE bottle, after shaking 2 h the aluminium source dissolved. Then, 9.54 g TEOS was added and followed by shaking and hydrolyzing the reactants for 24 h. In the next step, 0.18 g, 0.018 g and 0.0018 g (dry weight) S1 seeds were added to the clear solution for the synthesis of ZSM-5 crystals with thicknesses of ca 35, 105 and 253 nm, respectively. After adding seeds, the suspension was vigorously shaken for 1 h, and then cooled to 4 °C. At last, HF (about 1.13 g) was added quickly in an equimolar amount to TEAOH under stirring. After about 10 s, a very viscous white gel formed. The molar composition of the gel was 12TEAF: 25SiO_2: 0.417Al_2O_3: 500H_2O: 2.5i-PrOH: 100EtOH (the seed crystals are omitted). The gels with seeds were hydrothermally treated at 175 °C for 48 h in a 50 mL Teflon lined autoclave. The ZSM-5 crystals prepared in high yield were recovered by centrifugation and dispersion in distilled water for 4 times and freeze-dried. These crystals are denoted F35, F105 and F253.

2.4. ZSM-5 crystals with thicknesses of ca 28 nm grown in hydroxide medium (OH28)

ZSM-5 crystals with a thickness of ca 28 nm (OH28) was prepared as reported by Gevert et al. [24]. A mixture of 17.3 g TEOS, 14.82 g TPAOH (40% solution in water, Sigma) and 14.82 g H_2O was shaked for 15 h to hydrolyze the TEOS in a 100 mL PE bottle. 0.25 g Sodium aluminate (Aldrich, technical, anhydrous, Al (Al_2O_3): 50–56%, Na (as Na_2O): 40–45%) was dissolved at 70 °C in 4.19 g distilled water and the solution was filtered and added to the mixture, resulting in a synthesis solution with a molar composition of 8.75 TPAOH: 25 SiO_2: 0.417 Al_2O_3: 0.45 Na_2O: 466 H_2O: 100 EtOH. The solution was aged under reflux at 98 °C by heating in a silicon oil bath for 2 h. Then, the mixture was transferred to a 100 mL Teflon lined stainless steel autoclave and heated to 160 °C for 15 h. The crystals prepared in high yield were recovered by centrifugation and re-dispersion in distilled water four times and freeze-dried.

2.5. ZSM-5 crystals with thicknesses of ca 112, 185 and 391 nm grown in hydroxide medium (OH112, OH185 and OH391)

ZSM-5 crystals were prepared by adding S1 seeds to a 30 g gel with the composition: 25SiO_2: 12TEAOH: 500H_2O: 0.417 Al_2O_3 2.5i-PrOH: 100EtOH. The dry weight of added amounts of seeds were 0.018 g, 0.18 g and 1.0 g, for catalysts OH391, OH185, and OH112, respectively. After adding seeds, the dispersion was homogenized by shaking for 1 h, and then hydrothermally treated in a 50 mL autoclave at 180 °C for 4 days. The yield of crystals was not high, and after synthesis, the crystals were recovered by centrifugation at reduced speed resulting in an acceleration of 21,612 g and dispersion in distilled water 6 times and freeze dried. Centrifugation was carried out at reduced speed to separate the crystals from amorphous material.

2.6. Ion-exchange

All ZSM-5 catalysts were calcined at 550 °C for 6 h in ambient air. The crystals OH28 were ion-exchanged to the ammonium form in a 10 wt% NH_4NO_3 solution by dispersing 6 wt% crystals and heating the solution to 100 °C for 1 h under reflux with stirring.

The crystals were separated by centrifugation and re-dispersed in fresh NH_4NO_3 solution and again heated to 100 °C for 1 h under reflux with stirring. Finally, the crystals were separated by centrifugation, freeze dried and calcined at 550 °C for 6 h in ambient air.

3. Catalyst characterization

3.1. N_2 physisorption

Nitrogen adsorption/desorption isotherms was measured at −196 °C using a Micromeritics ASAP 2010 instrument. The samples were dried at 300 °C under vacuum overnight prior to analysis. Specific surface areas were computed by applying the Brunauer Emmet Teller (BET) and the Barrett Joyner Halenda (BJH) methods.

3.2. Morphological evaluation

The samples were imaged by scanning electron microscopy (SEM) without any coating using a Magellan XHR-SEM (FEI Company) instrument. The average thickness (T) of crystals, i.e. crystal length in the *b*-direction, was determined by measuring the thickness of at least 20 crystals from representative SEM images of each batch. This thickness was used as a key parameter when comparing catalysts. In order to verify the validity of the determined thickness, the specific external area $A_{external}$ of the crystals was estimated from the width (W), length (L) and thickness (T) estimated from SEM images and the density ($\rho_{zeolite}$) of ZSM-5 zeolite crystals, i.e., 1.76×10^6 g/m^3 as follows:

$$A_{external} = 2 \times W \times L + 2 \times L \times T + 2 \times W \times T/(W \times L \times T \times \rho_{zeolite}) \quad (1)$$

Since T is the smallest dimension, $A_{external}$ will be strongly dependent on T.

The specific internal area of the zeolite pores in ZSM-5 crystals was estimated from:

$$A_{internal} = S_{BET} - A_{external} \quad (2)$$

In this equation, S_{BET} is the specific surface area estimated by the BET method from nitrogen adsorption data at −196 °C, see below. Since $A_{internal}$ should be the area of zeolite pores, it should be constant for all samples if the estimated W, L and in particular T are reasonably correctly determined. The external area could also have been determined using a *t*-plot. However, the external area was instead estimated from the dimensions of the crystals and the internal area was estimated from equation (2) in order to establish if the dimensions are reasonably correctly determined.

3.3. XRD

X-ray diffraction (XRD) data were recorded using a Panalytical Empyrean diffractometer equipped with a high-resolution Cu X-ray tube and a Pixcel 3D detector. The instrument was operated in Bragg-Brentano geometry in the 2θ range 5-35° using fixed slits.

3.4. IR

FT-IR spectra were collected in transmission mode using a Bruker Vertex 70 instrument, equipped with a MCT detector. A home-made quartz cell, equipped with KBr windows and with an optical path of ca 2 mm was used. Samples were measured in the form of self-supporting pellets protected by a gold envelope. Before all IR measurements, the sample pellets were first heated to 500 °C under vacuum (residual pressure < 10^{-3} mbar) for 1 h. Then they were kept at the same temperature for an additional hour in an atmosphere of 50 mbar O_2 in order to oxidize any residual organic molecules and outgassed again under vacuum at the same temperature for another hour. After the sample activation, the cell was cooled at room temperature, maintained under vacuum and inserted in the IR measurement chamber. IR spectra were collected by accumulating 32 scans at 2 cm^{-1} resolution at "beam temperature" (the temperature reached under the IR beam, i.e. around 50 °C).

Adsorption of pyridine was performed to quantify the acid sites of the materials. Before each measurement of pyridine adsorption, sample pellets were weighted on an analytical balance and their geometric area was measured, in order to evaluate their optical density. Then after activation, they were exposed to pyridine vapor pressure at room temperature. The excess of adsorbed pyridine was removed by vacuum outgassing and then the pellets were heated at 200 °C for 1 h under dynamic vacuum to leave in interaction with the material only the strongly adsorbed pyridine. IR spectra were recorded after all the steps. The number of sites titrated by pyridine on self-supporting pellets was estimated integrating the IR bands at 1545 cm^{-1}and at 1455 cm^{-1} due to the analytical 19b vibrational modes of pyridine adsorbed on strong Brønsted Acid Sites (BAS) and on Lewis Acid Sites (LAS), respectively. The concentration of acid sites referred to the unit weight of sample has been computed according to the equations reported earlier [23] and considering the molar extinction coefficients reported by Nesterenko et al. [25]. The band deconvolution of the IR spectra was carried out using the FIT routine by Bruker, which allows the interactive research of the best fit to the examined experimental spectral segment on the basis of a number of spectral components imposed by the operator. All the major spectral parameters (spectral position, half-bandwidth, percent of Gaussian profile) were allowed floating freely.

3.5. Raman

UV-Raman spectra were collected with a Renishaw inVia Raman Microscope spectrometer, equipped with a Coherent MotoFred 300C frequency doubled Ar + laser emitting at 244 nm as excitation source, a 15x objective, a 3600 lines/mm grating and a Peltier cooled CCD detector. An home-made setup was exploited to avoid the degradation of coke under the highly energetic laser beam [26].

3.6. Temperature programmed desorption of NH_4 (NH_4TPD)

Desorption of ammonia was measured using a Micromeritics TPD/TPR 2900 analyzer. The samples were first heated to 823 K for 30 min under a flow of helium using a heating rate of 10 K/minute. In the next step, the samples were cooled to 473 K and flushed with ammonia for 10 min and then by helium for 10 min. Flushing with ammonia and helium was repeated three times in total. After observing a stable base line, ammonia was desorbed by heating the samples to 823 K using a heating rate of 10 K/minute.

3.7. Elemental analysis

The elemental compositions of the samples were measured by inductively coupled plasma – sector field mass spectrometry (ICP-SFMS, ALS Analytica, Luleå, Sweden). The samples were first melted in $LiBO_2$ and then dissolved in HNO_3 prior to analysis.

3.8. Methanol conversion to hydrocarbons

The catalysts were mixed with milled sand (Sigma-Aldrich, sea sand) in a weight ratio of 1:50 and loaded in a steel reactor (inner diameter 20 mm and length 250 mm). First, the catalysts were heated from room temperature to 400 °C during 90 min in a flow

of nitrogen. Then, nitrogen saturated with methanol at 18 °C was fed to the reactor at 400 °C to arrive at a WHSV of 8 g methanol/(g catalyst· h). The reactor effluent was analyzed approximately every 70 min using an online gas chromatograph (GC). The GC (Agilent 7890B) was equipped with a capillary column (CP-Sil PONA CB, 100 m × 250 μm × 0.5 μm, 37 psi) and a FID detector. After injecting the sample on the column at a split ratio of 30, the column temperature was kept at 30 °C for 5 min followed by a ramp of 5 °C/min to 180 °C, and the column was then held at this temperature for 9 min. A second ramp of 10 °C/min to 200 °C was then followed by a final hold time for 15 min to condition the column. The methanol peak was well separated from the DME peak. Common practice in the field is to not consider DME as a product when evaluating the methanol conversion, and this practice was followed in the present work.

4. Results and discussion

4.1. Characterization of ZSM-5 crystals

Fig. 1 (left) shows a SEM image of the S1 silicalite-1 seed crystals prepared using fluoride as mineralizing agent. The crystals display a leaf like habit with a length (*c*-direction) and thickness (*b*-direction) of most crystals typically<50 and 10 nm, respectively. By careful characterization using SEM, TEM, DLS, XRD, solid-state [29] Si MAS NMR, and adsorption/desorption experiments using nitrogen, water, *n*-butanol, and ethanol as adsorbates, we previously showed that these crystals are single crystals with significantly reduced number of structural defects in the lattice, i.e. "defect free", and increased hydrophobicity as compared to silicalite-1 crystals prepared using hydroxide as mineralizing agent [22].

Fig. 1 (right) illustrates the effect of different structure directing agents (SDAs) on the growth of S1 seeds. The use of TPAF as SDA gives rise to twin crystals with a thickness of ca 200 nm in the *b*-direction, as reported previously [20]. If TPAF is employed as SDA in combination with NH_4Br, the growth in the *a*/*c*- plane prevails, and the thickness in the *b*-direction is reduced to about 100 nm, but twinning is still observed. The growth of b-oriented aluminium free MFI films on seeded supports using TEAF as structure directing agent has been reported earlier [27]. The authors stated that the TEA + ion alone cannot act as a structure-directing agent to initiate self-nucleation of MFI crystals in the gel, but it can readily engender growth of MFI seed crystals when combined with a fluoride source. This work inspired us, and finally, as reported in the present paper, we observe that the use of TEAF mainly promotes growth in the *a*/*c*-plane, with the formation of ultrathin single crystals with a size (L × W × T) of about 400 × 100 × 35 nm. These crystals are denoted F35 from now on and are by far the thinnest ever reported ZSM-5 crystals grown in fluoride medium [20,28–34], as illustrated in Table 1. The low thickness observed in the present work is primarily a result of the use of the S1 silicalite-1 single crystals, with a thickness of only 10 nm in the *b*-direction, as seeds [21], and of an appropriate SDA to maintain the single crystalline nature, and avoid formation of twin crystals and mostly promote growth in the a/c- plane.

Fig. 2a shows a SEM image of the S1 crystals at lower magnification. Fig. 2b, c, d show SEM-images of ZSM-5 crystals grown in fluoride medium using S1 seed crystals and TEAF as SDA. These crystals are very well-defined and the average thicknesses T in the *b*-direction are 35, 105 and 253 nm, for samples F35, F105 and F253, respectively. The measured thickness varies, and the standard deviation is high, but the difference in average T between the different samples is sufficiently large for non-overlapping populations, see Table 2.

Fig. 2e shows a SEM image of the ZSM-5 crystals prepared in hydroxide medium, according to the method described by Gevert et al. [24]. The crystals are comprised of well-defined aggregates of much smaller crystals with a rectangular cuboid habit, with well-defined width (W), length (L) and thickness (T). The average thickness T is as small as about 28 nm, determined by measuring the thickness in the *b*-direction of at least 10 crystals in representative SEM images. For simplicity, these crystals are from now on denoted OH28. However, the thickness of the crystals varies significantly, and the standard deviation is as large as 8 nm; the length and width of these crystals are roughly 60 and 45 nm, respectively see, Table 2.

Fig. 2f, g, h show SEM images of ZSM-5 crystals prepared by seeding a hydroxide synthesis mixture with S1 seeds. These crystals have also a well-defined habit, and the larger crystals display the classical coffin-shape. The average thicknesses T in the *b*-direction determined from SEM images are 112, 185 and 391 nm, and consequently the samples are denoted OH112, OH185 and OH391, respectively. Table 2 shows that although the standard deviation is high, the populations do not overlap.

XRD data for all catalysts are shown in Fig. 3. Only reflections typical for the MFI phase are detectable and no signal from amorphous material is observed. A significant peak broadening is observed for the smallest crystals, as expected.

The specific BET surface area of samples was computed starting from the isotherms reported in Fig. S1. It ranges from 426 m^2/g for the smallest crystals (OH28) to 350 m^2/g for the largest (OH391) crystals, see Table 2. The much larger area measured for the smallest crystals should be an effect of larger external surface area. The external surface area was estimated for crystals with cuboid habit with dimensions W, L and T and the density of ZSM-5 zeolite, i.e., 1.76×10^6 g/m^3 as given by Equation (1) (see experimental section). For the smallest crystals OH28, the external surface area of the catalyst is as large as 85 m^2/g. It agrees well with the external BJH surface area of mesopores of 93 m^2/g as determined from the nitrogen adsorption data. The internal surface area, i.e., the surface area of ZSM-5 zeolite micropores, can be estimated to 341 m^2/g, by subtracting the estimated external surface area from the measured BET surface area using Equation (2) (see experimental section). Consequently, the external/internal surface area ratio is roughly as high as 85/341 ≈ 25% for this sample. For the other samples, internal surface areas in the vicinity of 350 m^2/g are also estimated, see Table 2. This is close to the expected surface area of 350 m^2/g for large ZSM-5 crystals with negligible specific external surface area (similar to the measured BET surface area for the largest crystals in the present work, i.e., OH391). This indicates that the estimated external dimensions, i.e. W, L and especially T of these crystals are correct. Since T is the smallest dimension of the crystals, it has the strongest influence on the estimated external surface area.

The Si/Al ratio and the corresponding Al concentration of the crystals as determined by ICP-SFMS are listed in Table 3. For the OH28, F35, F105 and F253 samples, the Si/Al ratio is close to 30, which is similar to the actual ratio in synthesis mixture. In contrast, the OH112, OH185 and OH391 samples have a higher ratio of about 55, although the actual Si/Al ratio in the synthesis mixture was 30. The corresponding concentration of Al expressed as μmol Al per gram of catalyst, computed from the zeolite stoichiometry by considering the above reported Si/Al ratios, are reported in the third column of Table 3.

The quantification of both Brønsted (BAS) and Lewis (LAS) acid sites was performed by means of IR spectroscopy, employing pyridine (Py) as the molecular probe, as described in detail in the experimental section. This molecule can be employed to detect and discriminate between LAS and BAS located inside the microchannels of the MFI framework. Indeed, it interacts with

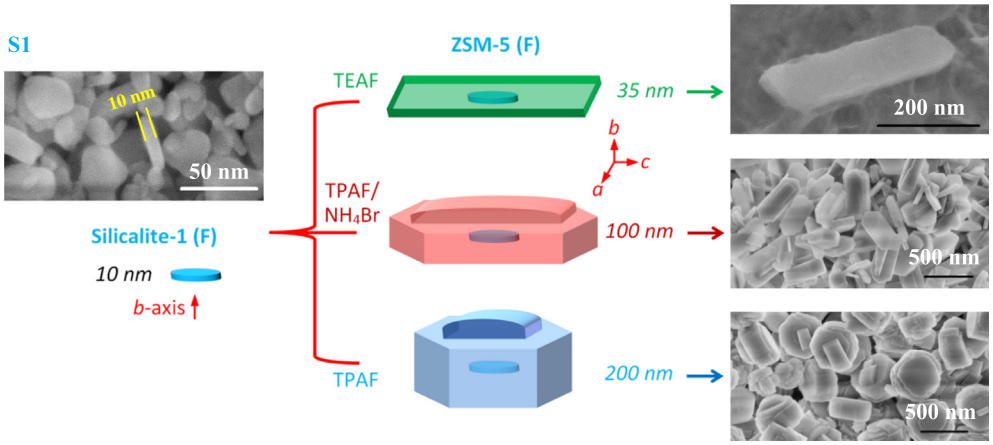

Fig. 1. SEM image of the S1 silicalite-1 seed crystals prepared using fluoride as mineralizing agent (left) and schematic illustration of growth of ZSM-5 crystals in fluoride media using TEAF (evaluated as catalysts), TPAF/ NH_4Br and TPAF as SDA from the 10 nm thick silicalite-1 seeds S1. Except for the different SDAs, the synthesis conditions are the same in all three cases (right).

Table 1
Comparison with ZSM-5 catalysts reported in the literature.

No	Application	Composition	Si/Al	T_{seed} (nm)	T_{ZSM-5} (nm)	Ref
1	MTH[a]	$82.23SiO_2$:$1Al_2O_3$:$5.56Na_2O$:$2.36TPABr$:$1373{\cdot}5H_2O$	15–140	–	500	[28]
2	CO_2 to gasoline	NA (commercial)	54–600	–	200	[29]
3	MTG[b]	$xNaAlO_2$:$100SiO_2$:$25TPAOH$:$1157H_2O$ (x = 0.5 ~ 8)	46–822	–	100	[30]
4	MTP[c]	$1.23Na_2O$:$9.74TPAOH$:$1Al_2O_3$:$43.2SiO_2$:$806H_2O$	25–35	–	100	[31]
5	MTH	$0.142TPABr$:$0.135TPAOH$:$0.072Al_2O_3$:$1SiO_2$:$0.616NH_4F$:$20H_2O$		80	200	[20]
6	MTP	$0.07TPABr$:$0.07TPAOH$:$1TEOS$:$0.01NaAlO_2$:$80H_2O$:$1.12NH_4F$		70	100	[32]
7	MTP	$1SiO_2$:$0.02Al_2O_3$:$0.048TPABr$:$0.8NH_4F$:$6H_2O$		–	100	[33]
8	MTH	$0.1TPAOH$:$1.0SiO_2$:$0.01Al_2O_3$:$0.8NH_4F$:$30H_2O$	72	–	100	[34]
9	MTG	$12TEAF$:$25SiO_2$:$0.417Al_2O_3$:$500H_2O$	35	10	35	Present work

[a] MTH (Methanol to hydrocarbons).
[b] MTG (Methanol to gasoline).
[c] MTP (Methanol to propylene).

strong Lewis acid sites and, in the presence of Brønsted acid centers, it undergoes protonation thanks to its high proton affinity. The IR spectra employed for the acid sites titration are reported for all samples in Fig. S2, in the spectral region of Py ring vibrational modes. The band located at 1450 cm^{-1} (identified in the Figure by a triangle) is employed for the quantification of Lewis acid sites, whereas the spectral component at 1550 cm^{-1} (identified in the Figure by a square), generated by the protonated Py, is related to the presence of acid sites with Brønsted character. The results of the quantification procedure are summarized in Table 3. The total concentration of acid sites (Lewis and Brønsted) is also computed, adding the amount of Lewis sites to the amount of Brønsted centers detected by Py. It is worth noting that, for all catalysts, the total acid sites concentration is in good agreement with the amount of Al derived from the stoichiometry. The maximum difference is observed for sample F105, for which an 18% higher total acid site concentration is observed as compared to the concentration estimated by ICP, illustrating the reliability of the quantification procedure performed with Py.

Beside to the evaluation of the total amount of acid sites, it is worth analyzing the population of Lewis and Brønsted sites of the catalysts. Indeed, despite the very similar amount of total acid sites, the materials synthesized in fluoride medium have a higher number of acidic sites with Brønsted character, with a clear trend: F35 < F105 < F253. Moreover, all samples (both F- and OH–) contain a fraction of strong Lewis acid sites due probably to the presence of some extra-framework Al species. In the catalysts obtained in fluoride media, the concentration of Lewis sites seems to have an opposite trend compared to the population of Brønsted sites, i.e exhibiting the minimum value in the material with the largest crystals: F35 > F105 > F253. In general, the catalysts obtained by the conventional synthesis possess less Brønsted sites, except for the material with the lowest crystals T (OH28) which has a concentration of Brønsted sites similar to the samples of the F- series. This difference could derive from the different synthetic procedure adopted for the OH28 sample.

Ammonia temperature programmed desorption data (NH_4TPD) is shown in Table 3. The observed ammonia desorption differs<10% compared to the Al concentration for the first four samples (OH28, OH112, O185 and OH391) in the Table. This indicates that ammonia is adsorbing selectively on the Al acid sites in the zeolite in a 1/1 ratio, as expected. However, for the three last samples (F35, F105 and F253), the ammonia desorption differs up to 30% from the measured Al concentration. For sample F35, a much lower ammonia desorption than the Al concentration was observed, while a much higher desorption than the Al concentration was observed for samples F105 and F253. This indicates that the quantification of acid sites performed by pyridine adsorption and IR spectroscopy is more reliable than NH_4TPD. Consequently, the former quantification is used in the following discussion.

Fig. 4 reports the IR spectra of all samples after activation at 500 °C in the region of the OH stretching vibrations and normalization to the zeolite overtones modes. IR spectra are grouped considering the crystals T: F35 and OH28 (T < 50 nm), F105, OH112 and

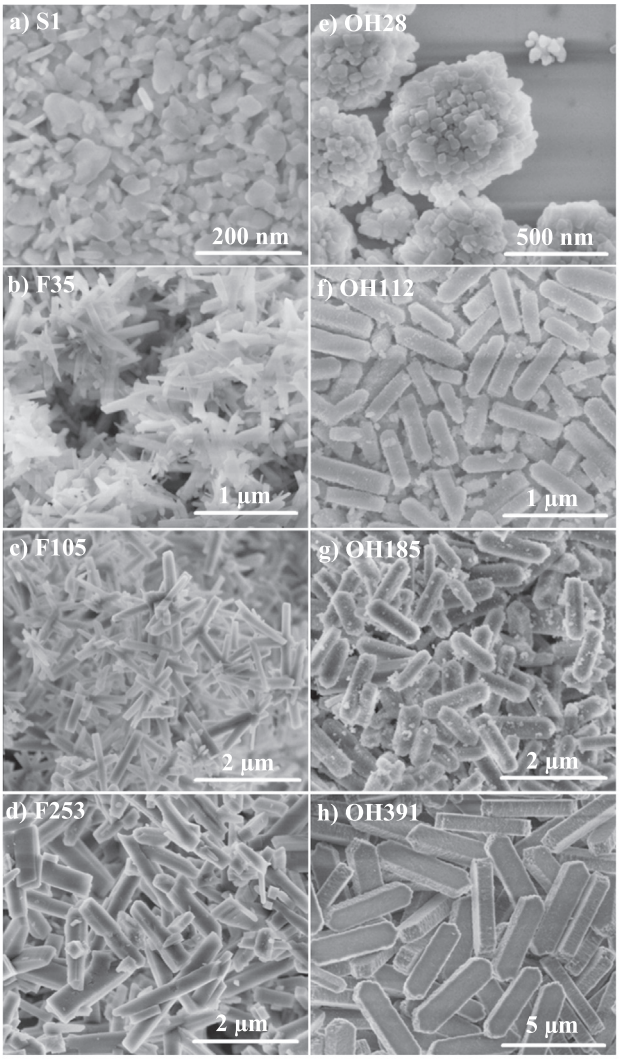

Fig. 2. SEM-images of a) silicalite-1 crystals S1 grown in fluoride medium, ZSM-5 crystals b) F35, c) F105, d) F253 grown in fluoride medium using TEAF as SDA, and ZSM-5 crystals e) OH28, f) OH112, g) OH185, h) OH391 grown in hydroxide medium.

OH185 (100 nm < T < 200 nm), F253 and OH 391 (T > 200 nm). Different families of OH groups are recognizable, located on the external and internal surface of the zeolite crystals. In particular, three main signals characterize the spectral region at 3800–3550 cm^{-1}. The sharp band at 3745 cm^{-1} is ascribed to isolated SiOH groups located on the external surface of the zeolite: this component is more intense when the fraction of external surface area is higher, i.e. in samples with smaller crystal size. The IR vibrational mode generated by Brønsted Al(OH)Si sites is instead located at 3610 cm^{-1}. The spectral intensity of this component in the various catalysts seems in agreement with the quantitative data obtained by Py adsorption. The signal at 3664 cm^{-1} is finally ascribed to AlOH species, generated by extra-framework Al species with Lewis acid character. The intensity of the band located at 3664 cm^{-1} is apparently altered by the difference in the spectrum profile in the 3740–3400 cm^{-1} region. Missing [SiO_4] units (defects) in the zeolite framework give rise to hydroxylated cavities, also known as silanol nests. The presence of these chains of hydrogen-bonded hydroxyl groups produces specific IR bands in the 3740–3700 cm^{-1} range due to SiOH species in terminal position and a broad and unresolved signal with apparent maximum between 3500 and 3400 cm^{-1}, assigned to adjacent OH groups mutually interacting via hydrogen bonds. [35] The above-mentioned spectral features are present in the IR spectra of all samples of the OH– series (OH28, OH112, OH185 and OH391), regardless their crystals size, whereas are totally absent for F35, F105 and F253 catalysts. It means that the materials obtained following the fluoride route are virtually free from defects.

The UV-Raman spectra of the spent OH112 and F105 samples are reported in Fig. 5. The spectral profiles of the two samples are substantially different, testifying a different nature of the coke species causing their deactivation. The profile of sample F105 is, as a matter of fact, broader and less defined than that of the OH112 sample. The presence of more defined bands in the spectrum for sample OH112, as highlighted by vertical dotted lines, is a clear signature of molecular coke. In detail, peaks at 1475 cm^{-1}, 1380 cm^{-1} and 1350 cm^{-1} refer to small polycyclic aromatic hydrocarbon molecules (PAHs, recognized as fluorene, naphthalene and phenanthrene respectively) [36]. These are overlapped with the broad profile typical of amorphous carbon, which main signals are identified at around 1600 cm^{-1} (the so-called G band) and 1400 cm^{-1} (referred as D band) [37,38]. The amorphous carbon signals are instead the only observed in the F105 sample. These clear differences suggest as, in the defect-free materials, deactivation occurs by deposition of an external layer of bulk coke, and possibly also carbon species (as shown by Weckhuysen [8]) not detected by Raman, see Fig. 7c). These carbon species may be e.g. pentacene molecules, straight molecules comprising five benzene rings, for which the Raman signal is expected to be weaker than for smaller PAH molecules, since its electronic transitions are more displaced toward the visible [39], thus the resonant enhancement from UV excitation is not exploited. Conversely, in defective samples, additional molecular coke species (hosted in the wider cavities generated by internal defects) further contribute to the deactivation process.

4.2. Methanol conversion to hydrocarbons (MTH)

The catalytic performances of all catalysts were evaluated in the MTH reaction as reported in the experimental section.

Fig. 6 shows a GC-chromatogram of the reactor effluent taken when the reactor is loaded with the OH28 catalyst after 3 h on stream at 80% methanol conversion. At a first glance, the appearance of all other recorded GC-chromatograms are similar and the

Table 2
Morphological and textural properties of the catalysts.

Catalyst Code	T (nm)	W (nm)	L (nm)	S_{BET} (m^2/g)	$A_{external}$ (m^2/g)	$A_{internal}$ (m^2/g)
OH28	28 ± 8	45	60	426	85	341
OH112	112 ± 17	200	600	344	18	326
OH185	184 ± 29	250	1000	365	12	353
OH391	391 ± 79	600	4000	350	5	345
F35	35 ± 16	100	400	418	47	371
F105	105 ± 35	150	1000	385	20	365
F253	253 ± 76	300	2000	388	9	379

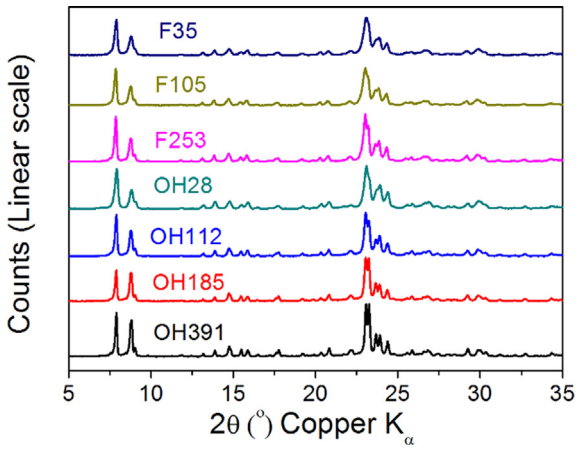

Fig. 3. XRD diffractograms for all catalysts in the 2θ range 5-35° recorded using CuKα radiation.

most prominent peaks are labelled in this chromatogram. However, as shown below, a closer inspection of the chromatograms reveals clear differences between the samples. The methanol peak at an elution time of 8.4 min is well separated from the DME peak at 8.1 min. The two largest product peaks are observed for propylene (7.8 min) and ethylene (7.5 min) and the propylene/ethylene carbon ratio is 2.75. The dominating aromatic compound and the third largest product peak is observed for pseudocumene, i.e. 1,2,4-trimethyl benzene (TMB), with a retention time of 33.3 min. Very low quantities of the other two TMB isomers 1,2,3-TMB (hemellitene) and 1,3,5-TMB (mesitylene) are observed.

For the OH28 catalyst after 3 h on stream at 80% methanol conversion, the 1,2,4-TMB/(total TMB) ratio is as high as 95%. From thermodynamic data [40], the 1,2,4-TMB/(total TMB) ratio at equilibrium is estimated to 66% at 400 °C. The much higher ratio observed experimentally than equilibrium suggests that mostly 1,2,4-TMB molecules escape the zeolite pores and that the other two isomers leave the pores in much lower quantities. As the external/internal surface area ratio is as high as 25% for this sample, the external area should be nearly inactive, due to very limited adsorption and/or coke formation at the surface. Indeed, if the external surface was very active, 1,2,4-TMB molecules formed in the zeolite pores should isomerize at the very large external surface of these small crystals and a composition closer to an equilibrium mixture of trimethyl benzenes should be observed in the effluent.

The second largest aromatic peak is observed for *m*-xylene with a retention time of 27.76 min. It is overlapping with the *p*-xylene peak with a retention time of 27.81 min. However, the two peaks were deconvoluted and integrated separately to evaluate the *p*-xylene yield. Finally, the heaviest compound detected in any significant quantity is durene (1,2,4,5-tetramethylbenzene) with a retention time of 38.4 min. The yield (carbon %) of durene is about 1% of all products formed for this sample. Even lower amounts of durene were detected for the other catalysts. It is worth repeating that up to about 4% durene is acceptable in gasoline fuel. Very small concentrations of isodurene (1,2,3,5-tetramethylbenzene) with a retention time of 38.6 min was detected and the durene/isodurene ratio was as high as 5.5. At equilibrium, a durene/isodurene ratio of 0.65 (i.e. the main product is isodurene) is expected at 400 °C as estimated from thermodynamic data. [39] Durene is selectively escaping the pores of ZSM-5[3] and the much higher ratio observed experimentally again indicates that the external surface is nearly inactive, due to low adsorption and/or coke formation. Indeed an active external surface would produce a ratio closer to equilibrium. Almost no signals for heavier compounds with retention time longer than 38.6 min (isodurene) were observed, as depicted in the inset of Fig. 6.

Fig. 7a reports methanol conversion as a function of time on stream for all catalysts. A high weight-hour-space-velocity (WHSV) of 8.0 g methanol/(g catalyst·h) was used in the present work, to observe deactivation within a convenient time of<100 h for all samples.

The F35 catalyst display superior performance with a methanol conversion exceeding 90% for the first 66 h on stream. However, after 66 h, deactivation is observed, and after about 91 h, 50% conversion is reached (see Fig. 7b). Previous reports on methanol conversion at comparable high space velocity are scarce, but Qin et al. [20] used a WHSV of 5.6 and observed an initial conversion of 84% for 200 nm thick crystals grown in fluoride medium. The higher conversion we observe at a higher space velocity highlights the advantage of 35 nm thick crystals in comparison to 200 nm thick crystals.

The two thicker catalysts prepared using fluoride as mineralizing agent (F105 and F253) display similar conversions higher than 90% during the first 5 h on stream. However, they start to deactivate after a much shorter time on stream and the time to reach 50% conversion is 43 h and 9 h, respectively. The much faster deactivation for crystals with the longest diffusion (F253) path should be an effect of higher sensitivity to percolation effects for larger crystals as suggested by Holmen et al. [10].

The three catalysts synthesized in fluoride medium have very similar Al concentration of about 450 μmol Al/g catalyst, whereas the average Al concentration for the other catalysts is about 400 μmol Al/g catalyst. In order to compensate for the slight variations in Al concentration, a normalized time to reach 50% conversion was estimated as follows:

Table 3
Concentration of acid sites in the catalysts.

Catalyst Code	Si/Al	μmol Al/g	Total acid sites from Py (μmol/g)	LAS from Py[a] (μmol/g)	BAS from Py[b] (μmol/g)	NH_3 desorpt. (μmol/g)
OH28	27.2	590	568	82	481	534
OH112	56.5	289	318	58	260	266
OH185	52.8	308	324	40	284	329
OH391	54.2	299	251	39	212	308
F35	33.7	474	436	64	372	337
F105	35.9	445	527	35	492	579
F253	35.4	450	518	19	499	530

[a] Calculated evaluating the integrated area of the analytical 19b mode of Py at 1455 cm^{-1} (in the dotted spectra of Fig. S2) and the integrated molar extinction coefficient reported in ref. 25, following the procedure reported in the experimental section.
[b] Calculated evaluating the integrated area of the analytical 19b mode of Py at 1545 cm^{-1} (in the dotted spectra of Fig. S2) and the integrated molar extinction coefficient reported in ref. 25, following the procedure reported in the experimental section.

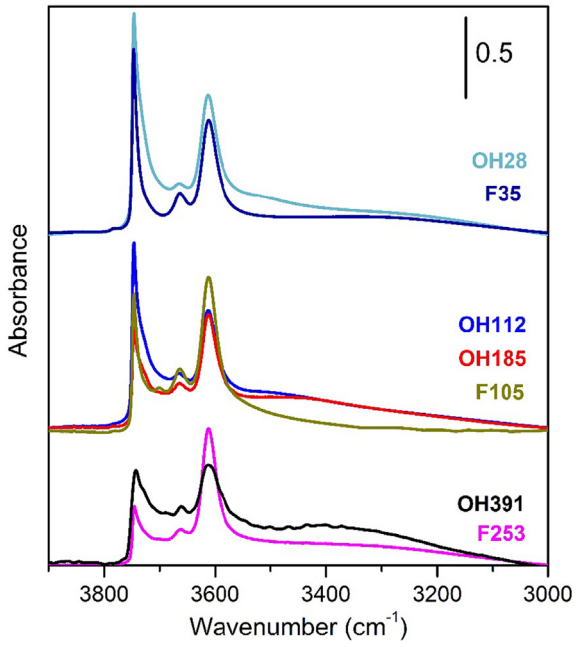

Fig. 4. IR spectra in the OH stretching region of the catalysts activated at 500 °C and normalized to the zeolite framework overtone modes.

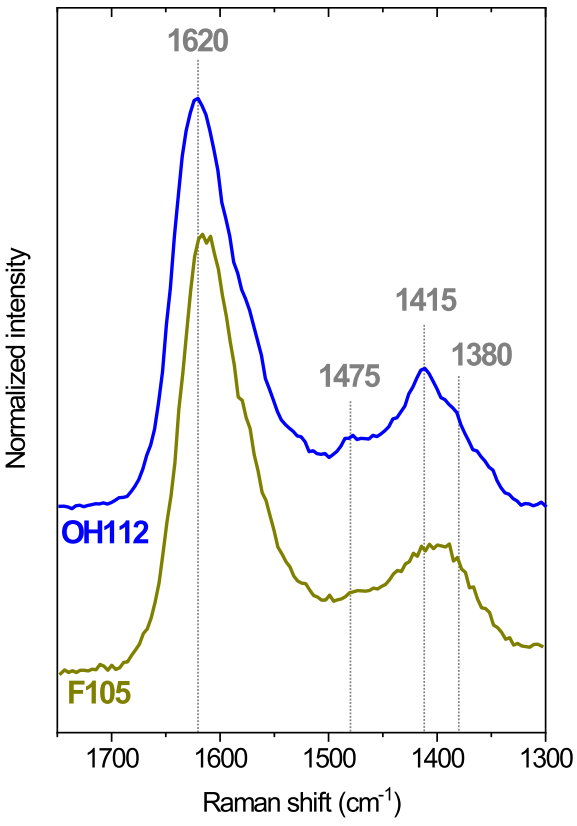

Fig. 5. UV-Raman spectra (λ = 244 nm) of spent samples OH112 and F105.

Normalized time to reach 50% conversion = Observed time to reach 50% conversion × 400 μmol Al/g sample/(observed Al concentration in μmol Al/g sample).

The normalized time to reach 50% conversion is approximately linearly proportional to the thickness T of the fluoride crystals, as indicated by dashed line in Fig. 7b.

The four catalysts OH28, OH112, OH185 and OH391 display high initial conversion in the early stages of the reaction (see Fig. 7a), higher than 75%, but significant deactivation is observed directly for all catalysts. In particular, catalyst OH28, with a crystal T and a Brønsted acid site concentration close to F35, starts to deactivate immediately and the deactivation continues progressively, illustrating the desirable catalytic properties of the defect free F35 sample. The normalized time to reach 50% conversion is almost linearly dependent of thickness T, and the correlation for OH catalysts is better (compared to the F catalysts) as indicated by a solid line in Fig. 7b. By comparing the two lines, it is clear that for comparable diffusion path, the defective crystals deactivate significantly faster than "defect free" crystals, for crystals with T < 200 nm. Indeed, as previously reported [23], samples synthesized in traditional hydroxyl medium deactivate faster due to the accumulation of molecular coke at the internal defects. The internal coke leads to percolation effects and increased diffusion resistance, resulting in faster deactivation.

In other words, as illustrated in Fig. 7c, likely only carbon species [8] form inside the micropores of defect free samples prepared using fluoride as mineralizing agent. In contrast, both carbon species and molecular coke generate in the microchannels of defective ZSM-5 crystals, giving rise to more extensive percolation effects and therefore to faster deactivation. In "defect free" crystals, bulk coke formation should occur only at the external surface of the particles, as bulk coke is much larger than the pores and cavities in defect free ZSM-5 [23]. However, the micropores of defect free ZSM-5 may very well accommodate small carbon species as suggested earlier [8]. Indeed, after a long time on stream, both small and large defect free and defective crystals may eventually deactivate also by external bulk coke formation. The faster deactivation of larger crystals (also if defect free) is related to significant diffusion limitations, coke formation and percolation effects [10]. However, external bulk coke formation will eventually deactivate also small defect-free catalysts, which would explain the strikingly slow deactivation of F35 crystals.

The yield (carbon %) of 1,2,4-TMB formed as a function of time on stream for the catalysts is reported in Fig. 7d. For the three catalysts with the lowest T, i.e. OH28, F35 and F105, the 1,2,4-TMB yield is initially very high due to the very short diffusion path. The 1,2,4-TMB yield first slightly increases, due to the time needed to fully build up the hydrocarbon pool in the catalyst. However, after a long time on stream, the 1,2,4-TMB yield eventually decreases, likely due to increased diffusion resistance as a result of formation of carbon species or molecular coke in the pores. For the four catalysts with the longest diffusion path, i.e. OH112, OH185, OH391 and F253, the 1,2,4-TMB yield is initially much lower, and decreases rapidly with time on stream. This indicates that these large crystals deactivate quickly by internal molecular coke (for defective catalysts OH112, OH185 and OH391) or carbon species [8] (defect-free F253) formation, which lead to increased internal diffusion resistance by percolation effects, and decreased 1,2,4-TMB yield.

The yield (carbon %) of 1,2,4-TMB formed initially and at 80% conversion as a function of T is shown in Fig. 8a. The initial 1,2,4-TMB yield and the yield at 80% conversion is similar for all catalysts but it varies significantly after longer time on stream when the conversion is further reduced (not shown for the sake of brevity). A very strong correlation of 1,2,4-TMB yield with T is observed and the crystals with the shortest diffusion path (F35 and OH28) produced more 1,2,4-TMB than the crystals with the longest diffusion path (F253 and OH391). This indicates that 1,2,4-TMB forms in the zeolite micropores and, consequently, higher yield is observed for crystals with short diffusion path, which allows the bulky 1,2,4-TMB molecule to more easily escape from the pores. There is a clear difference between defect free and

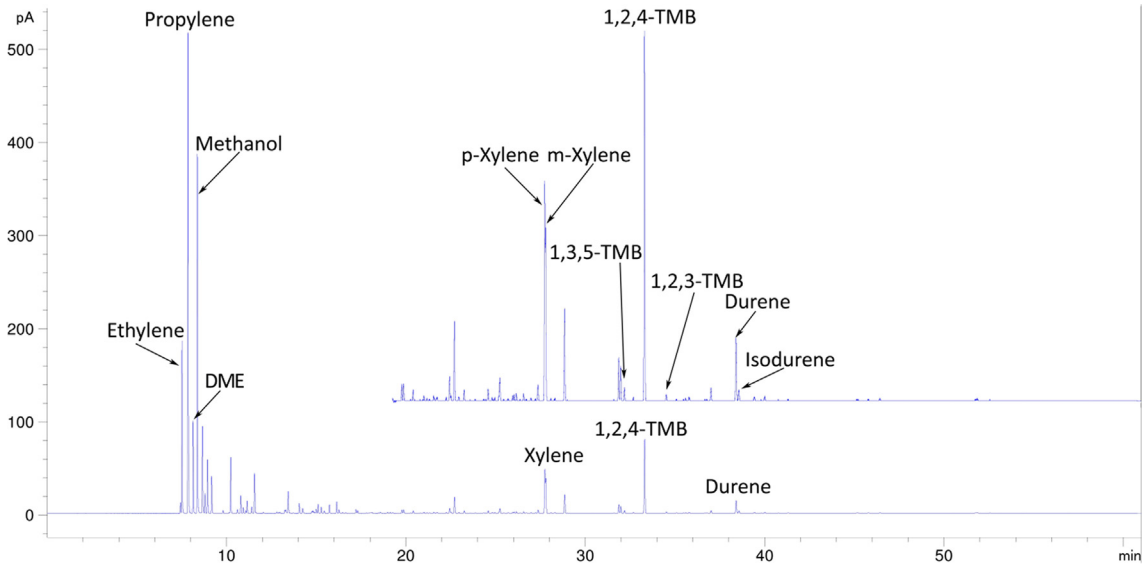

Fig. 6. GC-chromatogram taken from the reactor effluent when loaded with catalyst OH28 at 80% conversion after 3 h on stream. The inset shows the last part of the chromatogram with a 5 times magnified *y*-axis.

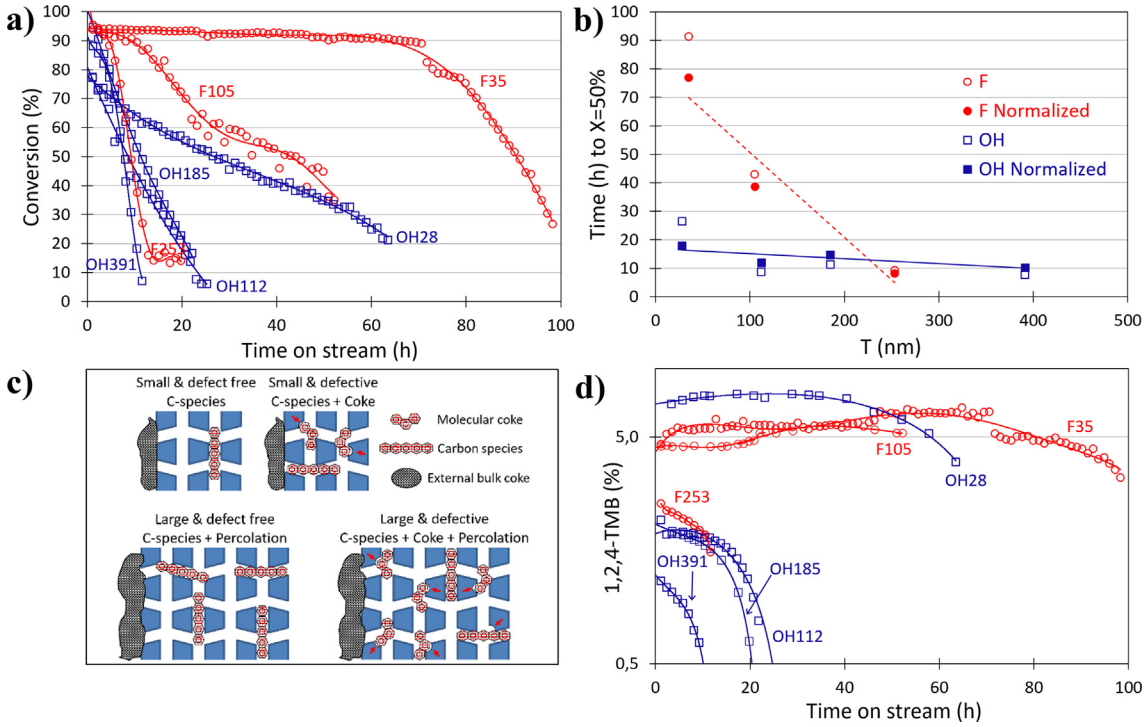

Fig. 7. a) Methanol conversion as a function of time on stream; b) time (h) to reach X = 50% as a function of thickness T for catalysts prepared using fluoride (F) and hydroxide (OH); c) schematic drawing illustrating deactivation of defect free and defective crystals by formation of external bulk coke, carbon species in the pores[8] and molecular coke in defects; d) yield of 1,2,4-TMB (carbon %) as a function of time on stream. Lines or curves are inserted in a), b) and d) to guide the eye.

defective catalysts for comparable diffusion path in the approximate range 50 < T < 250 nm. In this range, the defect-free crystals produce significantly more 1,2,4-TMB, likely due to less or no molecular coke formation in the pores.

The 1,2,4-TMB/(TMB) isomer ratio as a function of thickness T is given in Fig. 8b. Very high ratios, well above equilibrium (66% at 400 °C as estimated from thermodynamic data. [40]) are observed. The detection limit is about 99.5%, and even higher ratios are observed for samples F253 and OH391. At comparable T, this ratio is much higher for defect-free crystals. The other two isomers 1,2,3-TMB (hemellitene) and 1,3,5-TMB (mesitylene) probably mostly form in low quantities by isomerisation of 1,2,4-TMB at the nearly inactive external surface, probably due to an insignificant adsorption and coke formation. It explains why much higher ratios than equilibrium (66%) are observed. As discussed above, a much higher durene/isodurene isomer ratio than equilibrium was also observed. The observed trend for the durene/isodurene ratio as a function of thickness T was comparable to the trends of the 1,2,4-TMB/(TMB) isomer ratio as a function of T (not shown). Con-

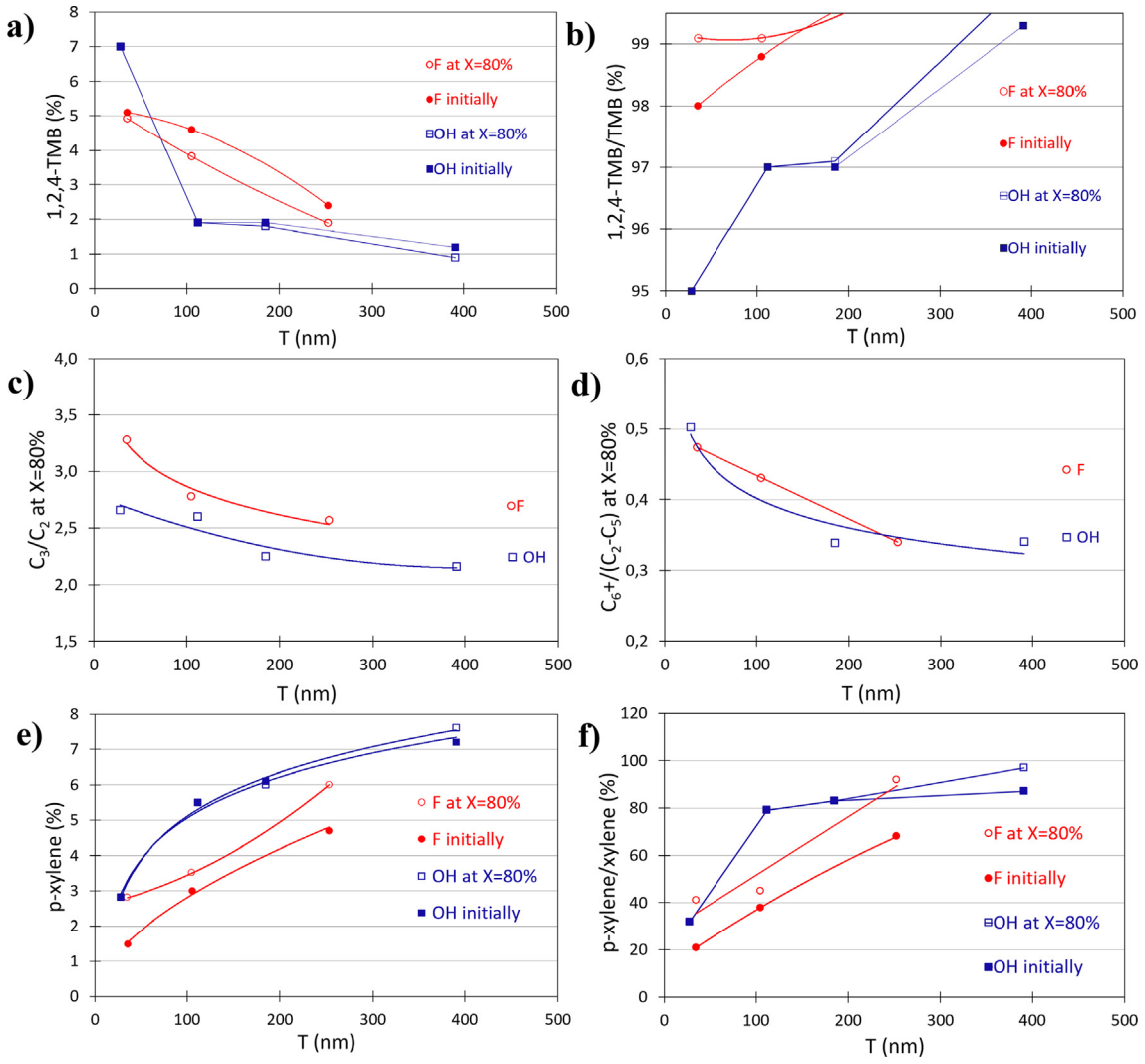

Fig. 8. a) Yield (carbon%) of 1,2,4-TMB and b) 1,2,4-TMB/(TMB) isomer ratio, initially and at 80% conversion, c) Propylene/ethylene carbon ratio observed at 80% conversion, d) $C_{6+}/(C_2\text{-}C_5)$ carbon ratio, e) Yield (carbon%) of *p*-xylene and f) *p*-xylene/xylene isomer ratio, initially and at 80% conversion, as a function of T for catalysts prepared using fluoride (F) and hydroxide (OH). Lines are inserted to guide the eye.

sequently, the observations for TMB isomers are supported by similar results for durene isomers.

The propylene/ethylene carbon ratio as a function of T is illustrated by Fig. 8c. A strong correlation with the shortest diffusion path is observed. The ratio is almost linearly inversely proportional to T and the highest ratio is observed for the crystals with the shortest diffusion path. It means that propylene can escape more easily from crystals with short diffusion path and low diffusion resistance. These results are in line with the observations of Bleken and co-workers [17] about the high C_3/C_2 carbon ratio displayed by MFI nanosheets, as compared to regular crystals.

Furthermore, a clear difference is observed between the defective and defect-free crystals. For comparable T, the defective crystals display lower propylene/ethylene ratio, indicating more diffusion resistance due to the presence of additional molecular coke in the micropores, as similarly observed for the 1,2,4-TMB yield.

The $C_{6+}/(C_2\text{-}C_5)$ carbon ratio, i.e. the gasoline/light component ratio, is strongly correlated to the thickness of the crystals and is shown in Fig. 8d. Crystals with the shortest diffusion path produced a significantly higher fraction of gasoline (C_{6+}) than crystals with longer diffusion path. The heavier gasoline molecules can more easily escape from crystals with low diffusion resistance and short diffusion path. Defect-free crystals displayed a higher ratio, in the rough range 50 nm < T < 250 nm, further indicating no formation of molecular coke in these crystals. The high yield of gasoline and 1,2,4-TMB with high octane number in combination with very slow deactivation illustrate the potential of thin and defect free crystals reported herein for gasoline synthesis.

The yield of *p*-xylene as a function of T is reported in Fig. 8e. As *p*-xylene is a component with relatively high diffusivity in ZSM-5 compared to 1,2,4-TMB, totally opposite trends are observed for the *p*-xylene yield, as compared to the 1,2,4-TMB yield. Crystals with larger T result in higher yield of *p*-xylene and, for comparable T, defect-free crystals with presumably lower diffusion resistance due to less molecular coke formation in the pores, results in lower *p*-xylene yield, as expected. The *p*-xylene/xylene isomer ratio is shown in Fig. 8f. The equilibrium ratio is estimated to 24% at 400 °C from thermodynamic data. [40] The smallest crystals prepared using fluoride (F35) initially displays a ratio of 20%, i.e. very close to equilibrium. However, after 54 h on stream, when the conversion has been reduced to 80%, the ratio more than doubles. It proves that the diffusion resistance of the crystals is increasing, as a result of carbon species formation in these defect-free crystals.

As the ratio is controlled by diffusion resistance, and all three xylene isomers form in, and escapes from, the zeolite pores, the ratio is increasing with increasing T. Defective crystals display higher ratios at comparable T, likely due to molecular coke formation and increased diffusion resistance. A very high ratio exceeding 90% is observed for the largest OH391 crystals, at 80% conversion. By extrapolating the results for fluoride crystals, it seems that fluoride crystals with a thickness of about 400 nm would give equally high ratio. The trends on the *p*-xylene/xylene isomer ratio are in sharp contrast to the 1,2,4-TMB/TMB isomer ratio (Fig. 8b), for which defect-free crystals display a higher ratio than defective crystals. This indicates that the isomers 1,2,3-TMB and 1,3,5-TMB are mostly formed in very low quantities at the nearly inactive external surface, while the *m*- and *o*-xylene isomers form in, and escape, the zeolite micropores.

5. Conclusions

In the present work, two sets of defect free and defective ZSM-5 crystals with controlled thickness (T) between 30 and 400 nm and similar Si/Al ratio and acid site density were synthesized employing different synthetic routes. For the first time, ZSM-5 crystals with thickness down to 35 nm, prepared in fluoride medium by using silicalite-1 crystals as seeds, were synthesized, investigated and evaluated for methanol conversion. These small, defect free crystals exhibited excellent catalytic activity in methanol conversion, giving high yield of gasoline. The two sets of samples were fully characterized and compared, allowing a complete and new systematic investigation on the influence of the crystal thickness and the presence or absence of defects on the catalytic performances of H-ZSM-5 during methanol conversion. A well-known protocol of characterization (largely used for the characterization of acidic zeolites) was exploited, to extensively investigate the active sites nature and abundance. Consequently, the role played by internal defects and thickness on catalytic performances was finally disclosed.

Although the external/internal surface area ratio was as high as 25% for the smallest crystals, only low concentrations of compounds likely mostly forming on the surface of the zeolite (1,2,3-TMB, 1,3,5-TMB, 1,2,3,5-tetramethylbenzene and heavier compounds) were detected in the reactor effluent. This indicates that the external area of the catalysts is almost inactive, probably due to very low adsorption and/or coke formation. Strong correlations between deactivation rate and the shortest diffusion path, i.e. crystal thickness, were observed. Crystals with large thickness, i.e. longer diffusion paths, deactivated much faster than crystals with short diffusion path. The deactivation should be caused by molecular coke and/or carbon species formation in the pores and percolation effects, the latter having a larger influence on crystals with long diffusion path. For crystals with comparable thickness, defect free crystals deactivated much slower. This phenomenon was assigned to no molecular coke formation in the microchannels of defect free crystals. It is possible that the defect free crystals only deactivate by internal carbon species formation and external coke formation. The faster deactivation of defective crystals is caused by additional internal molecular coke formation, not occurring in defect free crystals. The length of the shortest diffusion path was shown to strongly influence the 1,2,4-TMB yield, the TMB isomer ratio, the propylene/ethylene ratio, the $C_{6+}/(C_2\text{-}C_5)$ ratio, the p-xylene yield and the xylene isomer ratio. Crystals with short diffusion path favored the formation of heavier/slowly diffusing compounds (1,2,4-TMB, propylene (over ethylene) and C_{6+}). Oppositely, crystals with long diffusion path favored the formation of light/fast diffusing components (C_2–C_5 and *p*-xylene). For crystals with comparable shortest diffusion path, a higher yield of the heavy compounds (1,2,4-TMB, propylene and C_{6+}) was observed for defect free crystals, and this was assigned to less diffusion resistance due to less or no molecular coke formation in these crystals. For large crystals, the 1,2,4-TMB yield was initially low, and it further decreased with time on stream, presumably due to internal molecular coke and carbon species formation in defective and defect free crystals, respectively.

To summarize, the small defect free crystals with a thickness of 35 nm reported here, for the first time, displayed very good activity, stability and high selectivity to pseudocumene (with high octane number), gasoline and propylene. Consequently, these crystals seem ideal for gasoline synthesis. On the contrary, for high selectivity to *p*-xylene, larger crystals with a thickness of about 400 nm would be suitable, but these deactivate rapidly due to carbon species and/or molecular coke formation in the pores and percolation effects.

Declaration of Competing Interest

The authors declare that they have no known competing financial interests or personal relationships that could have appeared to influence the work reported in this paper.

Acknowledgment

Financial support from the Swedish Research Council (2014-04585_VR) and Bio4energy are acknowledged. Swedish Energy Agency is acknowledged by financing part of the work (O. Öhrman) through grant ID P41164-1.

Appendix A. Supplementary material

Supplementary data to this article can be found online at https://doi.org/10.1016/j.jcat.2022.04.013.

References

[1] U. Olsbye, S. Svelle, K.P. Lillerud, Z.H. Wei, Y.Y. Chen, J.F. Li, J.G. Wang, W.B. Fan, The formation and degradation of active species during methanol conversion over protonated zeotype catalysts, Chem. Soc. Rev. 44 (2015) 7155–7176.
[2] P. Tian, Y.X. Wei, M. Ye, Z.M. Liu, Methanol to olefins (MTO): from fundamentals to commercialization, ACS Catal. 5 (2015) 1922–1938.
[3] U. Olsbye, S. Svelle, M. Bjorgen, P. Beato, T.V.W. Janssens, F. Joensen, S. Bordiga, K.P. Lillerud, Conversion of methanol to hydrocarbons: how zeolite cavity and pore size controls product selectivity, Angew. Chem. Int. Edit. 51 (2012) 5810–5831.
[4] I. Yarulina, A.D. Chowdhury, F. Meirer, B.M. Weckhuysen, J. Gascon, Recent trends and fundamental insights in the methanol-to-hydrocarbons process, Nat. Catal. 1 (2018) 398–411.
[5] F.J. Keil, Methanol-to-hydrocarbons: process technology, Micropor. Mesopor. Mat. 29 (1999) 49–66.
[6] D. Rojo-Gama, M. Signorile, F. Bonino, S. Bordiga, U. Olsbye, K.P. Lillerud, P. Beato, S. Svelle, Structure-deactivation relationships in zeolites during the methanol–to-hydrocarbons reaction: complementary assessments of the coke content, J. Catal. 351 (2017) 33–48.
[7] K. Barbera, F. Bonino, S. Bordiga, T.V.W. Janssens, P. Beato, Structure-deactivation relationship for ZSM-5 catalysts governed by framework defects, J. Catal. 280 (2011) 196–205.
[8] J.E. Schmidt, J.D. Poplawsky, B. Mazumder, Ö. Attila, D. Fu, D.A.M. de Winter, F. Meirer, S.R. Bare, B.M. Weckhuysen, Coke formation in a zeolite crystal during the methanol-to-hydrocarbons reaction as studied with atom probe tomography, Angew. Chem. Int. Edit. 55 (2016) 11173–11177.
[9] A.O.E. Beyne, G.F. Froment, A percolation approach for the modeling of deactivation of zeolite catalysts by coke formation: diffusional limitations and finite rate of coke growth, Chem. Eng. Sci. 48 (1993) 503–511.
[10] D. Chen, H.P. Rebo, A. Holmen, Diffusion and deactivation during methanol conversion over SAPO-34: a percolation approach, Chem. Eng. Sci. 54 (1999) 3465–3473.
[11] a) A.A. Rownaghi, J. Hedlund, Methanol to gasoline-range hydrocarbons: influence of nanocrystal size and mesoporosity on catalytic performance and product distribution of ZSM-5, Ind. Eng. Chem. Res. 50 (2011) 11872–11878.
[12] A.A. Rownaghi, F. Rezaei, J. Hedlund, Yield of gasoline-range hydrocarbons as a function of uniform ZSM-5 crystal size, Catal. Commun. 14 (2011) 37–41.

[13] M. Zhou, A.A. Rownaghi, J. Hedlund, Synthesis of mesoporous ZSM-5 zeolite crystals by conventional hydrothermal treatment, RSC Adv. 3 (2013) 15596–15599.
[14] D. Chen, K. Moljord, T. Fuglerud, A. Holmen, The effect of crystal size of SAPO-34 on the selectivity and deactivation of the MTO reaction, Micropor. Mesopor. Mat. 29 (1999) 191–203.
[15] B.P.C. Hereijgers, F. Bleken, M.H. Nilsen, S. Svelle, K.P. Lillerud, M. Bjørgen, B.M. Weckhuysen, U. Olsbye, Product shape selectivity dominates the methanol-to-olefins (MTO) reaction over H-SAPO-34 catalysts, J. Catal. 264 (2009) 77–87.
[16] M. Choi, K. Na, J. Kim, Y. Sakamoto, O. Terasaki, R. Ryoo, Stable single-unit-cell nanosheets of zeolite MFI as active and long-lived catalysts, Nature 461 (2009) 246–249.
[17] B.T.L. Bleken, D.S. Wragg, B. Arstad, A.E. Gunnaes, J. Mouzon, S. Helveg, L.F. Lundegaard, P. Beato, S. Bordiga, U. Olsbye, S. Svelle, K.P. Lillerud, Unit cell thick nanosheets of zeolite H-ZSM-5: structure and activity, Top. Catal. 56 (2013) 558–566.
[18] J.M. Chezeau, L. Delmotte, J.L. Guth, Z. Gabelica, Influence of synthesis conditions and postsynthesis treatments on the nature and quantity of structural defects in highly siliceous MFI zeolites: a high-resolution solid-state ^{29}Si NMR study, Zeolites 11 (1991) 598–606.
[19] F.L. Bleken, S. Chavan, U. Olsbye, M. Boltz, F. Ocampo, B. Louis, Conversion of methanol into light olefins over ZSM-5 zeolite: strategy to enhance propene selectivity, Appl. Catal. A-Gen. 447 (2012) 178–185.
[20] Z.X. Qin, L. Lakiss, L. Tosheva, J.P. Gilson, A. Vicente, C. Fernandez, V. Valtchev, Comparative study of nano-ZSM-5 catalysts synthesized in OH^- and F^- media, Adv. Funct. Mater. 24 (2014) 257–264.
[21] M. Zhou, J. Hedlund, Facile preparation of hydrophobic colloidal MFI and CHA crystals and oriented ultra-thin films, Angew. Chem. Int. Ed. 57 (2018) 10966–10970.
[22] H. Zhou, J. Mouzon, A. Farzaneh, O.N. Antzutkin, M. Grahn, J. Hedlund, Colloidal defect-free silicalite-1 single crystals: preparation, structure characterization, adsorption, and separation properties for alcohol/water mixtures, Langmuir 31 (2015) 8488–8494.
[23] M. Grahn, A. Faisal, O.G.W. Öhrman, M. Zhou, M. Signorile, V. Crocellà, M.S. Nabavi, J. Hedlund, Small ZSM-5 crystals with low defect density as an effective catalyst for conversion of methanol to hydrocarbons, Catal. Today 345 (2020) 136–146.
[24] B. Gevert, L. Eriksson, A. Torncrona, Preparation of discrete colloidal ZSM-5 crystals with high Al-content, J. Porous Mat. 18 (2011) 723–728.
[25] N.S. Nesterenko, F. Thibault-Starzyk, V. Montouilliout, V.V. Yushchenko, C. Fernandez, J.-P. Gilson, F. Fajula, I.I. Ivanova, The use of the consecutive adsorption of pyridine bases and carbon monoxide in the IR spectroscopic study of the accessibility of acid sites in microporous/mesoporous materials, Kinet. Catal. 47 (2006) 40–48.
[26] M. Signorile, F. Bonino, A. Damin, S. Bordiga, A novel Raman setup based on magnetic-driven rotation of sample, Top. Catal. 61 (2018) 1491–1498.
[27] C.T.P. Tung, H.S. Kim, K.B. Yoon, Growth of uniformly oriented silica MFI and BEA zeolite films on substrates, Science 334 (2011) 1533–1538.
[28] N.L. Michels, S. Mitchell, J. Perez-Ramirez, Effects of binders on the performance of shaped hierarchical MFI zeolites in methanol-to-hydrocarbons, ACS Catal. 4 (2014) 2409–2417.
[29] J. Wei, Q.J. Ge, R.W. Yao, Z.Y. Wen, C.Y. Fang, L.S. Guo, H.Y. Xu, J. Sun, Directly converting CO_2 into a gasoline fuel, Nat. Commun. 8 (2017) 15174.
[30] Z.J. Wan, W. Wu, G. Li, C.F. Wang, H. Yang, D.K. Zhang, Effect of SiO_2/Al_2O_3 ratio on the performance of nanocrystal ZSM-5 zeolite catalysts in methanol to gasoline conversion, Appl. Catal. A-Gen. 523 (2016) 312–320.
[31] A. Palcic, V.V. Ordomsky, Z.X. Qin, V. Georgieva, V. Valtchev, Tuning zeolite properties for a highly efficient synthesis of propylene from methanol, Chem. Eur. J. 24 (2018) 13136–13149.
[32] J.J. Li, M. Liu, X.W. Guo, C.Y. Dai, C.S. Song, Fluoride-mediated nano-sized high-silica ZSM-5 as an ultrastable catalyst for methanol conversion to propylene, J. Energy Chem. 27 (2018) 1225–1230.
[33] L.L. Zhang, Y. Song, G.D. Li, Q. Zhang, S.L. Zhang, J. Xu, F. Deng, Y.J. Gong, F-assisted synthesis of a hierarchical ZSM-5 zeolite for methanol to propylene reaction: a *b*-oriented thinner dimensional morphology, RSC Adv. 5 (2015) 61354–61363.
[34] W. Dai, C. Kouvatas, W. Tai, G. Wu, N. Guan, L. Li, V. Valtchev, Platelike MFI crystals with controlled crystal faces aspect ratio, J. Am. Chem. Soc. 143 (2021) 1993–2004.
[35] M. Signorile, V. Crocellà, A. Damin, B. Rossi, C. Lamberti, F. Bonino, S. Bordiga, Effect of Ti speciation on catalytic performance of TS-1 in the hydrogen peroxide to propylene oxide reaction, J. Phys. Chem. C 122 (2018) 9021–9034.
[36] M. Signorile, F. Bonino, A. Damin, S. Bordiga, In situ resonant UV-Raman spectroscopy of polycyclic aromatic hydrocarbons, J. Phys. Chem. C 119 (2015) 11694–11698.
[37] A.C. Ferrari, J. Robertson, Resonant Raman spectroscopy of disordered, amorphous, and diamondlike carbon, Phys. Rev. B 64 (7) (2001) 075414.
[38] A.C. Ferrari, J. Robertson, Interpretation of Raman spectra of disordered and amorphous carbon, Phys. Rev. B 61 (20) (2000) 14095–14107.
[39] M. Zander, UV atlas of organic compounds, 1967, 3, E4/1.
[40] D.R. Stull, G.C. Sinke, E.F. Westrum, The Chemical Thermodynamics of Organic Compounds, Malabar, Fla., Krieger, 1987.